On the Reaction Path Hamiltonian for Polyatomic Molecules†

Javier González,‡,|| Xavier Giménez,‡,|| and Josep Maria Bofill*,§,||

Departament de Química Física, Departament de Química Orgànica, and Centre Especial de Recerca en Química Teòrica, Universitat de Barcelona, Martí i Franquès 1, E−08028 Barcelona, Catalunya, Spain

Received: October 16, 2000; In Final Form: February 21, 2001

The classical reaction path Hamiltonian formulation of Miller, Handy, and Adams is reformulated using a linear expansion of the gradient in internal coordinates. It leads to a correspondence between the arc length, *s*, along the intrinsic reaction coordinate, and the whole set of internal coordinates and, furthermore, to a dynamical equation for *s*, a second-order Bernoulli-type equation, which is analytically solvable inside the validity range of the quadratic expansion of the potential. Therefore, by virtue of the above correspondence, the time dependence of the whole set of internal coordinates is easily recovered, by means of a few functional and overlap evaluations. It thus enhances the computational performance of the overall direct dynamics method. The unimolecular 1,2 hydrogen migration, between the (corresponding) carbene and ethyne oxide, is considered as example for illustrative purposes.

I. Introduction

Much progress has been made recently on accurate theoretical treatments of the dynamics of molecular systems.[1] Powerful classical, semiclassical, and quantum mechanical techniques, combined with the availability of impressive computational resources, have led to a number of interesting applications. These range from essentially exact treatments of triatomic systems to approximate, but fairly accurate, studies of large polyatomic molecules, including processes such as electronic nonadiabatic transitions, reactions at surfaces, solvent effects, cluster rearrangements, etc.[1]

In practical terms, though, two main difficulties still arise when performing such ab initio studies. The first one is the computation of the potential energy surface, which has to be, frequently, fitted to an analytical function. As the dimensionality of the system increases, so does, exponentially, the number of quantum chemistry calculations necessary to cover the configuration space. Also involved is the fit to the analytical function. The second difficulty, which bears a common origin with the first one, is the exponential increase in computational effort needed to explore the nuclear dynamics of these increasingly complex systems. The previously quoted advances have certainly reduced the overall computational effort, yet the exponential growth of it still persists.

As a consequence, the specific search for approximate yet accurate methods for exploring the structure-plus-dynamics molecular problem is remarkably intense. An appealing idea, which intelligently synthesized some interesting previous efforts,[2] was set forth by Miller, Handy, Adams in 1980,[3] when the reaction path Hamiltonian (RPH) was proposed. It exploits the fact that, in the course of a rearrangement, a path is described in going from reactants to products that is sufficiently close to the minimum energy path (MEP). Therefore, some kind of "guidance" exists and just a given portion of configuration space is preferentially sampled. This combines with the fact that efficient algorithms were developed for such MEP following in standard quantum chemistry calculations. The result is that the number of structure calculations is reduced to that corresponding to the MEP, plus a normal-mode analysis performed at each relevant point along it.

The RPH ideas were consistently completed by formulating the Hamiltonian for the nuclear motion in terms of the *reaction path coordinate system*.[2,3] The issue of developing suitable coordinate systems for the description of dynamical problems is ubiquitous in molecular science.[1] It became especially relevant for treating chemical reactions, because, usually, a rearrangement process renders inefficient an important class of the most common coordinate systems, e.g. those tied to one of the arrangements. The RPH formulation can thus be viewed as an effort along this line, that directly accounts for the fragment reorganization leading to chemical reaction. The RPH is then expressed in terms of an arc length, along the MEP, plus $3N - 7$ normal mode vibrational coordinates orthogonal to it, where N is the number of atoms.

Central to the final RPH expression are the "couplings", i.e., matrix elements that are ultimately responsible for the energy transfer between each degree of freedom.[3,4] In any other formulation, the energy transfer taking place among degrees of freedom, thanks to the PES topography, is actually "hidden" in its usually obscure dependence on each coordinate. Conversely, the RPH couplings show these transfers more explicitly, thus reflecting the importance of the reaction path curvature, as well as any change in the vibrational mode features, as one advances along the reaction coordinate. Overall, one obtains a chemically sound way of incorporating the dynamics in the description of a reaction mechanism. In addition, with the use of a RPH, one may expect that the essential items of a reactive process are taken into account, whereas the less essential parts may be treated accurately by either factoring them out or including them by means of approximate methods. Actually, both the description of structural features and the development of more or less approximate dynamical theories, under the reaction path philosophy, have been actively pursued by a number of workers.[5] Especially interesting have been the efforts in recasting the

† This paper is dedicated to Prof. William H. Miller on the occasion of his 60th anniversary.

* Corresponding author. E-mail: jmbofill@qo.ub.es
‡ Departament de Química Fisica.
§ Departament de Química Orgànica.
|| Centre Especial de Recerca en Química Teòrica.

10.1021/jp003793k CCC: $20.00
Published on Web 05/01/2001

transition state theory within the context of the reaction path Hamiltonian.[6]

The Miller, Handy, Adams (MHA) dynamical formulation makes use throughout of expanding the interaction potential up to second order, the role of the couplings in the Hamiltonian being an immediate consequence of it. This well-known technique has been used in other contexts as the basis for the formulation of full dynamical methods[7,8] and has proven effective for alleviating the computational effort, while being reasonably accurate. Actually, the original RPH method considers expanding the potential up to quadratic terms *for all coordinates but one*, the arc length (s) being left out from this expansion, because it is considered the associated motion to be far from harmonic (the original MHA work derived its formulation from the treatment of floppy-like modes). Then, one performs a parameter-dependent (on s) quadratic expansion. The treatment is unified a posteriori by including the effect of the reaction coordinate in the coupling matrix elements.[3]

The present work originated from the wish to treat the dynamics of very large molecular systems, for which direct dynamics methods appear to be more affordable (relatively speaking), when implemented within the RPH context. Our starting point has been to consider the quadratic expansion for *all* degrees of freedom, i.e., including in it the reaction coordinate s. However, the dynamically unique, central role played by s requires a specific formulation for the expansion. It has been found that, starting from the definition of the MEP—more precisely, the definition of the intrinsic reaction coordinate (IRC)—and performing a first-order expansion of the gradient, it is possible to establish a relationship between s and the complete set of internal coordinates. More important, this relationship leads to a constraint that, ultimately, translates into a dynamical equation for s and, in the classical Hamiltonian formulation, its conjugate momentum p_s. The appealing feature of the approach is that this equation of motion is *analytically solvable*, inside the validity range of the quadratic expansion, provided that the structural information (gradients and Hessians) is available at each required value of the reaction coordinate. A main result is that, at first instance, the couplings are not required for the solutions, i.e., the normal mode time dependence inside each quadratic expansion of the potential. Then, each quadratic solution couples to the next through the eigenvectors overlap between consecutive quadratic expansions, or further when recovering the Cartesian coordinate time dependence. One thus has analytic solutions that are stepwise corrected to get the final, continuous trajectories. The computational performance of the present RPH formulation is, consequently, enhanced, since obtaining the time dependence for each variable is a matter of just some functional plus some overlap evaluations.

The issue is then the global accuracy of the quadratic expansion for the reaction coordinate, e.g., how the neglect of the (seemingly important) anharmonicity terms really affect the final results. The algorithm actually implemented uses the standard procedure of defining the step size by monitoring the difference between the quadratic and the true potentials. Previous experience with this kind of approach tells that a reasonable accuracy might be expected for large molecular systems.[8] This should be the case for the present application because, as one increases the complexity of the molecular system, the easier it will be to find important departures from the harmonic behavior, for degrees of freedom other than the reaction coordinate, so that the anharmonicity of the latter should become less particular. In other words, one is forced, anyway, to define a small step size to keep the validity of the quadratic expansion. The present work intends to provide a test of this approximation.

The remainder of the paper is organized as follows. Section II describes the formulation of the equations resulting from the quadratic expansion, for all degrees of freedom, in the definition of the IRC. Section III describes the algorithmic implementation. Section IV presents some results of the application of the present dynamical model, and section V concludes.

II. Derivation of the Reaction Path Hamiltonian

Before considering an actual molecular system, it is useful to treat the reaction path formalism using the full set of internal coordinates, M, rather than the 3N Cartesian coordinates of the N atoms. The set of internal coordinates is $M = 3N - 6$, ($M = 3N - 5$ for diatomic molecules). It is well known that the reaction path is obtained by starting at a saddle point and performing calculations at a sequence of nuclear positions. This sequence is determined by following the normalized gradient vector, in mass-weighted internal coordinates,[9−11]

$$\mathbf{G}_0^{-1/2}\frac{d\Delta\mathbf{q}_0}{ds} = \frac{\Delta\underline{\mathbf{q}}_0}{ds} = \frac{\mathbf{G}_0^{1/2}\mathbf{g}(\Delta\mathbf{q}_0(s))}{\sqrt{[\mathbf{g}(\Delta\mathbf{q}_0(s))]^T\mathbf{G}_0\mathbf{g}(\Delta\mathbf{q}_0(s))}} = \frac{\underline{\mathbf{g}}(\Delta\underline{\mathbf{q}}_0(s))}{\sqrt{[\underline{\mathbf{g}}(\Delta\underline{\mathbf{q}}_0(s))]^T\underline{\mathbf{g}}(\Delta\underline{\mathbf{q}}_0(s))}} \quad (1)$$

where $\Delta\mathbf{q}_0 = \mathbf{q} - \mathbf{q}_0$ and $\mathbf{g}$ are M-dimensional internal coordinates and gradient vector, respectively. $\mathbf{G}_0$ is Wilson's G-matrix[12] of dimension M × M, evaluated at $\mathbf{q}_0$. The $\Delta\underline{\mathbf{q}}_0$ and $\underline{\mathbf{g}}$ vectors denote the corresponding mass-weighted internal coordinates and gradient, respectively. The first-order differential eq 1 defines the tangent of the IRC[9] in internal coordinates, whereas the parameter s plays the role of an arc length. The above IRC is a parametrically defined curve in the M-dimensional mass-weighted internal coordinate space[13]

$$\underline{\mathbf{q}} = \underline{\mathbf{q}}(s) = \{\underline{\mathbf{q}}_1(s), ..., \underline{\mathbf{q}}_M(s)\}^T \quad (2)$$

The variation of the potential energy surface, $V(\underline{\mathbf{q}})$, along the IRC line is then found to be

$$\frac{dV(\underline{\mathbf{q}})}{ds} = \mathbf{g}^T\frac{d\Delta\underline{\mathbf{q}}_0}{ds} = \sqrt{\mathbf{g}^T\mathbf{g}} \quad (3)$$

showing that the energy surface is parametrically dependent on the arc length, s. The calculation of the gradient vector and the Hessian matrix is nowadays relatively easy in any quantum chemistry calculation. Consequently, it has been proposed that eq 1 be integrated by successive local quadratic approximation algorithms.[14−17] Sun and Ruedenberg[17,18] noted that the solution to

$$u\frac{d\Delta\underline{\mathbf{q}}_0(u)}{du} = \mathbf{g}(\Delta\underline{\mathbf{q}}_0(u)) \quad (4)$$

gives a IRC path identical to that obtained from eq 1 and that eq 4 can be solved exactly when the potential energy is a quadratic function of the coordinates.

The connection between eq 1 and eq 4 is established by defining the parameter

$$u(s) = \exp\left[\int_{s_0}^{s}\frac{1}{\sqrt{\mathbf{g}^T\mathbf{g}}}ds'\right] \quad (5a)$$

then

$$\frac{du}{u} = \frac{1}{\sqrt{\mathbf{g}^T\mathbf{g}}}ds \tag{5b}$$

Now the mass-weighted potential energy gradient vector is expressed in the local quadratic approximation

$$\mathbf{g}(\Delta\mathbf{q}_0) = \mathbf{g}_0 + \underline{\mathbf{F}}_0\Delta\mathbf{q}_0 \tag{6}$$

where $\mathbf{g}_0$ and $\underline{\mathbf{F}}_0$ are, respectively, the gradient vector and Hessian matrix, in mass-weighted internal coordinates, represented at $\underline{\mathbf{q}} = \underline{\mathbf{q}}_0$. Equating eqs 4 and 6 and integrating the resulting equation leads to a piecewise quadratic approximation for the IRC path. The locally quadratic IRC curve, $\underline{\mathbf{q}}(u)$, is then

$$\underline{\mathbf{q}}(u) = \underline{\mathbf{q}}_0 - (\mathbf{I} - u^{\underline{\mathbf{F}}_0})\underline{\mathbf{F}}_0^{-1}\mathbf{g}_0 \tag{7}$$

where $\mathbf{I}$ is the unit matrix and the $u^{\underline{\mathbf{F}}}$ matrix is defined as

$$u^{\underline{\mathbf{F}}_0} = \mathbf{V}_0\{u^{f_i^0}\delta_{ij}\}\mathbf{V}_0^T \tag{8}$$

The orthogonal matrix of eigenvectors, $\mathbf{V}_0 = (\mathbf{v}_1^0| \ldots |\mathbf{v}_M^0)$, and the eigenvalues $\{f_i^0\}_{i=1}^M$ are obtained from the diagonalization of the mass-weighted Hessian matrix, $\mathbf{V}_0^T\underline{\mathbf{F}}_0\mathbf{V}_0 = \{f^0{}_i\,\delta_{ij}\}$.

Equation 7 is then the constraint that makes possible relating the set of M internal coordinates to the defined variable u. Substituting it into the local quadratic approximation of the potential energy surface around $\underline{\mathbf{q}}_0$, we obtain the analytical dependence of the potential energy on u, along the quadratic IRC curve. This expression is

$$V(u) = W_0 + \frac{1}{2}\mathbf{g}_0^T u^{\underline{\mathbf{F}}_0}\underline{\mathbf{F}}_0^{-1}u^{\underline{\mathbf{F}}_0}\mathbf{g}_0 \tag{9}$$

where

$$W_0 = V_0 - \frac{1}{2}\mathbf{g}_0^T\underline{\mathbf{F}}_0^T\mathbf{g}_0 \tag{10}$$

V_0 being the potential energy at $\underline{\mathbf{q}} = \underline{\mathbf{q}}_0$.

As u is now the generalized coordinate, by using its time evolution it is possible to evaluate the kinetic energy of a molecular system moving along the quadratic IRC path. In other words, we obtain the kinetic energy of a system moving along the curve defined in eq 4, constrained by eq 7, as a function of du/dt

$$T\left(\frac{du}{dt}, u\right) = \frac{1}{2}\left(\frac{d\Delta\underline{\mathbf{q}}_0}{dt}\right)^T\left(\frac{d\Delta\underline{\mathbf{q}}_0}{dt}\right) = \frac{1}{2}\left(\frac{d\Delta\underline{\mathbf{q}}_0}{du}\frac{du}{dt}\right)^T\left(\frac{d\Delta\underline{\mathbf{q}}_0}{du}\frac{du}{dt}\right) = \frac{1}{2}\underline{\mathbf{g}}_0^T u^{2(\mathbf{F}_0-\mathbf{I})}\underline{\mathbf{g}}_0\left(\frac{du}{dt}\right)^2 \tag{11}$$

Equation 7 has been used in the derivation of eq 11. Using both the kinetic energy given in eq 11 and the potential energy given in eq 9, we can build the Lagrange function, $L(u, du/dt; t)$,[19] corresponding to the same motion of the molecular system along the quadratic IRC path,

$$L(u, du/dt; t) = T(du/dt, u) - V(u) = \frac{1}{2}\mathbf{g}_0^T\left(u^{2(\underline{\mathbf{F}}_0-\mathbf{I})}\left(\frac{du}{dt}\right)^2 - u^{\underline{\mathbf{F}}_0}\underline{\mathbf{F}}_0^{-1}u^{\underline{\mathbf{F}}_0}\right)\underline{\mathbf{g}}_0 - W_0 \tag{12}$$

The curve $u = u(t)$ that makes stationary the functional

$$J[u] = \int_{t_0}^{t} L\left(u, \frac{du}{dt}; t\right) dt \tag{13}$$

is that satisfying the well-known Euler−Lagrange differential equation,[19] which in this case takes the form

$$\frac{d^2u}{dt^2} + u^{-1}\left(\frac{du}{dt}\right)^2\frac{\mathrm{Tr}(\underline{\mathbf{F}}_0 - \mathbf{I})}{M} + u = 0 \tag{14}$$

where Tr stands for a matrix trace. The IRC reaction path Hamiltonian is derived in the usual way,[19]

$$H(u, p_u; t) = p_u\frac{du}{dt} - L\left(u, \frac{du}{dt}; t\right) \tag{15}$$

where the conjugate momentum, p_u, is given by

$$p_u = \frac{\partial L}{\partial\left(\frac{du}{dt}\right)} = \mathbf{g}_0^T u^{2(\underline{\mathbf{F}}_0-\mathbf{I})}\mathbf{g}_0\frac{du}{dt} \tag{16}$$

Now using equations12, 15, and 16 we obtain the Hamilton function

$$H(u, p_u; t) = \frac{1}{2}\frac{p_u^2}{\mathbf{g}_0^T u^{2(\underline{\mathbf{F}}_0-\mathbf{I})}\mathbf{g}_0} + \frac{1}{2}\mathbf{g}_0^T u^{\underline{\mathbf{F}}_0}\underline{\mathbf{F}}_0^{-1}u^{\underline{\mathbf{F}}_0}\mathbf{g}_0 + W_0 \tag{17}$$

Note that no explicit representation of the angular momentum is considered in the present Hamiltonian. Actually, for large molecular systems, the rotational constants will be small. Consequently, the rotational periods will hardly match with those corresponding to vibration, so that the rotation−vibration coupling is expected to be small. In these cases, approximate, separable methods should be reasonable, inexpensive alternatives to account for the effect of rotation. Finally, note that by applying Hamilton's equations of motion to eq 17, one may recover, as expected, eq 14.

It proves convenient, for the integration of the differential eq 14, to use the transformation $u = \exp(\tau)$. The resulting equation is

$$\frac{d^2\tau}{dt^2} + \left(\frac{d^2\tau}{dt^2}\right)^2\left(\frac{\mathrm{Tr}(\underline{\mathbf{F}}_0 - \mathbf{I})}{M} + 1\right) + 1 = 0 \tag{18}$$

Now we apply the transformation $\chi = d\tau/dt$ to the above equation, obtaining

$$\frac{d\chi}{dt} + A\chi^2 + 1 = 0 \tag{19}$$

where $A = (\mathrm{Tr}(\underline{\mathbf{F}}_0 - \mathbf{I})/M + 1)$. Equation 19 is a second-order Bernoulli's differential equation. Its solution distinguishes three cases:

$$\text{(1) if } A > 0 \text{ then } u(t) = [C_2\cos(t\sqrt{A} + C_1)]^{1/A} \tag{20a}$$

$$\text{(2) if } A < 0 \text{ then } u(t) = [C_2\cosh(-t\sqrt{|A|} + C_1)]^{-1/[A]} \tag{20b}$$

$$\text{(3) if } A = 0 \text{ then } u(t) = \exp\left(-\frac{1}{2}t^2 + C_1t + C_2\right) \tag{20c}$$

Finally, we note that the present problem is similar to the "brachistochrone problem",[20] because in the present case the molecular system falls from the transition state to a minimum,

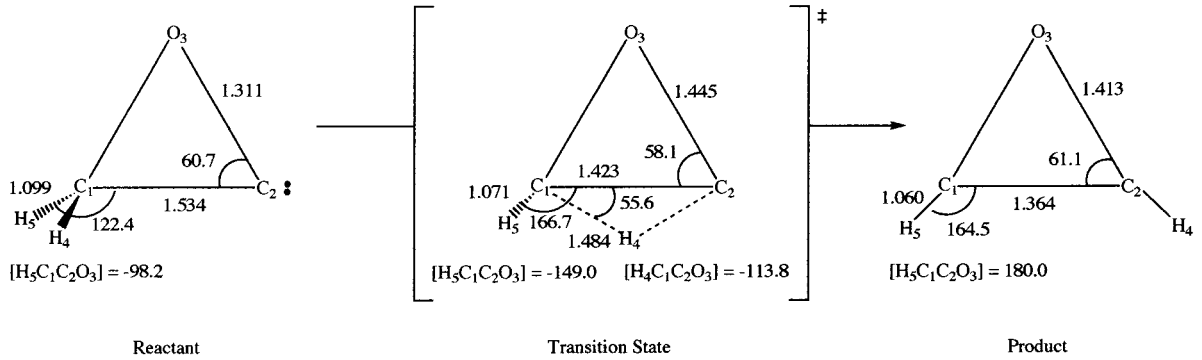

Figure 1. Schematic picture of the unimolecular rearrangement process studied in the present work, the 1,2 hydrogen migration between the (corresponding) carbene and ethyne oxide. Data in square brackets stand for dihedral angles, in their usual notation.

either reactant or product, on the potential energy surface, but is restricted to move along the IRC curve.

III. Algorithm

In this section we present a practical way to integrate the IRC path Hamiltonian, from the transition state to either reactant or product regions, by successive quadratic approximations. We assume that a transition state and the reactants and products minima have been located using standard methods,[21] the gradient vector and the Hessian matrix being available as well at any desired point along the IRC path. The Hessian matrix and the gradient vector are computed and transformed to internal coordinates, so as to build the present quadratic approximation. The most expensive part of this algorithm is the evaluation of the Hessian matrix. Nevertheless, it is possible to update the Hessian matrix using the Murtagh−Sargent−Powell formula,[22−24] rather than to compute it fully, even though this feature is not tested at present.

A brief description of the algorithm may be given as follows. At a point of the IRC, $\mathbf{q}_0$, compute the energy, gradient vector, and Hessian matrix. Both the gradient vector and the Hessian matrix are then transformed to internal coordinates, denoted by $\mathbf{g}_0$ and $\mathbf{F}_0$, respectively. Compute also the $\mathbf{G}_0$ matrix. Using eq 7, find a value of u such that the next inequality is satisfied:

$$[(\Delta\underline{\mathbf{q}}_0(u))^{\mathrm{T}}(\Delta\underline{\mathbf{q}}_0(u))]^{1/2} \leq R \tag{21}$$

where R is the "trust radius" that characterizes the trust region, i.e., the validity region for the current quadratic model. Employing the corresponding eq 20, we compute the time t, for the given value of u, that the system spends inside the current paraboloid. Note that at the beginning of each quadratic model, $u(0) = 1$ and $\mathrm{d}u(0)/\mathrm{d}t$ takes the value

$$\frac{\mathrm{d}u(0)}{\mathrm{d}t} = \frac{\mathbf{g}_0^{\mathrm{T}}\dfrac{\mathrm{d}\mathbf{q}_0}{\mathrm{d}t}}{\mathbf{g}_0^{\mathrm{T}}\mathbf{g}_0} \tag{22}$$

Equation 22 is obtained by differentiation of eq 7 with respect to time and imposing $u(0) = 1$. Using both $u(0) = 1$ and the above $\mathrm{d}u(0)/\mathrm{d}t$, we compute the C_1 and C_2 constants appearing in eq 20. The trust radius, R, is adjusted at each step according to the technique proposed by Culot et al.,[25] which has been used several times in optimization[22,25] and dynamic algorithms.[26] The velocity for each internal coordinate is then evaluated according to the equation

$$\frac{\mathrm{d}\underline{\mathbf{q}}}{\mathrm{d}t} = \underline{\mathbf{u}}^{\mathbf{F}_0^{-1}}\mathbf{g}_0\frac{\mathrm{d}u}{\mathrm{d}t} \tag{23}$$

This process is carried out until the reactant and product minima are reached.

The initiation step is performed at the transition state, where the gradient vector is equal to the null vector and, consequently, the basic eq 1 cannot be used strictly. However, it is possible to show, by application of L'Hôpital's rule, that the IRC curve converges to the transition vector, $\mathbf{v}^0_{\mathrm{ts}}$, at this point.[15] In other words, $\mathbf{g}_0/(\mathbf{g}_0{}^{\mathrm{T}}\mathbf{g}_0)^{1/2} \rightarrow \mathbf{v}^0_{\mathrm{ts}}$ at a first-order saddle point. By taking this result into account, eq 23 is reduced to $\mathrm{d}\underline{\mathbf{q}}/\mathrm{d}t = \mathbf{v}^0_{\mathrm{ts}}\,\mathrm{d}u/\mathrm{d}t$ (with $u = 1$). Consequently, only $\mathrm{d}u/\mathrm{d}t$ is required as input.

Finally, we note that in the region where the $\underline{\mathbf{F}}_0$ matrix is negative definite, eq 7 is not defined properly. In this case one should use the corresponding quadratic image function, so that the stability for the basic eq 7 is recovered.[27]

IV. Results and Discussion

The application of the present RPH implementation is illustrated here by considering a unimolecular rearrangement process, the 1,2 hydrogen migration between the (corresponding) carbene and ethyne oxide.[28,29] A scheme for this process is shown in Figure 1, where the equilibrium geometry for the transition state is shown explicitly.

The application of the present method to the above unimolecular process required first testing that the trust radius chosen for each quadratic step and the first-order expansion of the gradient lead to a converged description of the reaction path dynamics. Results of the final converged numerical parameters are shown in Table 1. Quite remarkably, only ca. 20 steps for each of the transition state (TS)-to-products or the TS-to-reactants IRC branches have been necessary for that converged description. This convergence was tested, as usual, by considering trust radius one-half of the original ones and then checking that the final results were invariant.

The present algorithm has been implemented in a computer code that has been interfaced to the MOPAC quantum chemistry package. The PES IRC points, plus the related gradient vectors and Hessian matrices, have been computed at the MNDO−UHF level.[30] The present system has been chosen, as stated, for illustrative purposes. Consequently, the accuracy of the PES is not our main goal in the present work. Rather, the present system has been chosen because it is a truly multidimensional (9-mode) problem with a PES that exhibits remarkable features. Figure 2 shows the potential profile for the above rearrangement process as a function of the IRC arc length s. In the figure, negative s values stand for the reactants region, whereas positive values correspond to products. This will be the case for the remaining figures, unless explicitly stated otherwise. The following IRC displays a barrier of ca. 65 kcal/mol, the rearrangement process being slightly exothermic by ca. 7 kcal/mol. According to the

TABLE 1: Numerical Parameters and Behavior of the Present Algorithm, as Applied to the Rearrangement of Ethyne Oxide[a]

step	R[b]	u[c]	s[d]	s_t[e]	t[f]	t_t[g]	cr[h]	gradient norm[i]
0	0.500	1.649	0.500	0.500	0.361	0.361	0.858	0.004
1	0.089	2.163	0.178	0.678	0.105	0.466	1.045	91.306
2	0.084	1.938	0.168	0.845	0.098	0.564	1.040	101.613
3	0.119	2.366	0.237	1.082	0.138	0.702	1.035	109.358
4	0.168	2.994	0.335	1.417	0.190	0.892	1.019	118.054
5	0.237	3.313	0.478	1.896	0.229	1.121	0.918	129.813
6	0.300	0.313	0.309	2.204	0.201	1.322	0.997	163.196
7	0.300	0.120	0.107	2.311	0.204	1.525	1.023	120.275
8	0.300	0.064	0.081	2.392	0.182	1.707	1.009	93.101
9	0.300	0.028	0.065	2.457	0.156	1.864	0.999	68.282
10	0.300	0.007	0.049	2.506	0.131	1.995	0.998	47.055
11	0.300	0.000	0.034	2.539	0.101	2.096	1.001	29.940
12	0.200	0.000	0.021	2.560	0.060	2.155	0.997	16.411
13	0.084	0.002	0.014	2.575	0.031	2.186	0.993	8.946
14	0.079	0.000	0.009	2.583	0.023	2.209	0.991	5.908
15	0.050	0.000	0.006	2.590	0.014	2.223	0.990	3.395
16	0.021	0.001	0.003	2.593	0.007	2.230	1.000	1.831
17	0.017	0.000	0.002	2.595	0.005	2.235	1.000	1.160
18	0.010	0.000	0.001	2.596	0.003	2.238	1.000	0.673
19	0.005	0.000	0.001	2.597	0.002	2.239	1.000	0.388

[a] Parameters correspond to those characterizing the path obtained starting at the transition state (TS) and proceeding downhill toward the product minimum. Similar data characterize the TS-reactants path. [b] R = trust radius, in bohr. [c] The u value is calculated according to eq 21. [d] s = arc length for each step. It is evaluated by integration of eq 5b, and given in amu$^{1/2}$ bohr. [e] The cumulative arc length, in amu$^{1/2}$ bohr. [f] The time step, in au, evaluated according to eq 20. [g] The cumulative time step, in au. [h] The validity of the current quadratic model is evaluated using the expression $\mathrm{cr} = \Delta E^{(2)}/(V(u) - V_0)$, where $V(u)$ is given in eq 9 and $\Delta E^{(2)}$ is the real quadratic variation of the potential energy. [i] The current gradient norm, in kcal mol^{-1} Å^{-1} − kcal mol^{-1} rad^{-1}.

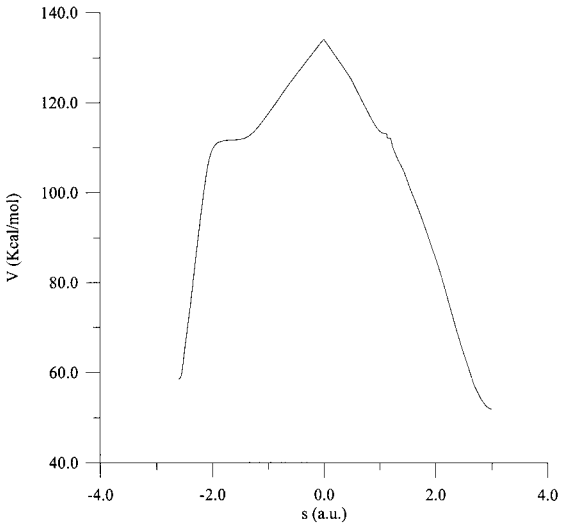

Figure 2. Potential energy profile along the IRC arc length s. Negative s values correspond to reactant configurations, whereas positive s values stand for products. Zero of s corresponds to the saddle point configuration. The maximum of the potential curve shows an apparent derivative discontinuity. It originates in the fact that the IRC equation is not defined at $s = 0$ (see discussion following eq 23). Consequently, the inner region corresponding to the first trust radius is not explored and, to avoid a discontinuous trace in the plot, just three potential values are calculated and further connected by straight lines.

barrier height value, significant mode excitation is to be expected for trajectories overcoming the potential barrier.

The IRC profile shows, in addition, two blips after the TS, at about $s = 1.1$, as well as a shoulder at about $s = -2$. They

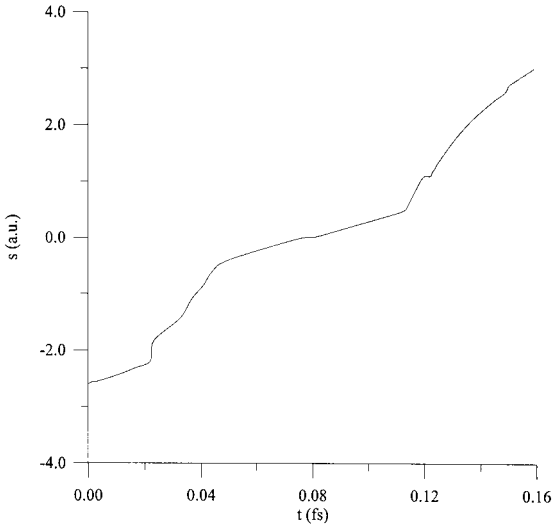

Figure 3. Time dependence of the IRC arc length s, as it is obtained from the solution of eq 14.

reflect the existence of bifurcation points along the IRC path. The first one, located in the reactants region, is found at an energy of 108.51 kcal/mol, and its geometry is slightly distorted from that shown in Figure 1 for the transition state, in the sense that H_4 is closer to C_1 (the C−H distance is now 1.245 Å). The second is located well in the products region, having an energy of 111.61 kcal/mol and displaying a geometry close to that shown in Figure 1 for the products configuration. The difficulties of the IRC following algorithms in such PES regions are well known. One could consider initially a system free of such features, for testing purposes. However, such difficulties in exploring PESs are more likely as the molecular system considered becomes more involved. Furthermore, the resulting dynamics is found to be not particularly affected, from the methodological point of view, by the fact that PES regions exhibiting bifurcation points are being sampled (see discussion below). Finally, the RPH philosophy is especially suited for large molecular systems, given the IRC following constraint, for the arc length coordinate, involved in its formulation. All of these reasons prompted us to consider such an involved system as a good candidate to test the present methodology.

The primary quantity obtained from the application of the present RPH formulation is the arc length time dependence, i.e., the solution of eq 19 and therefore of eq 14. It provides information on the dynamics of a point particle restricted to follow the IRC line. The s time dependence thus obtained is shown in Figure 3. As it can be seen, the highest accelerations roughly correlate to the strongest variations of the potential in Figure 2. However, the curvature effects and normal mode coupling, included in eq 14 through the gradient and the A factor, cause the s time dependence to be far from simple. Thus, even though the potential is strongly varying across the saddle point ($s = 0$), the velocity along s is lower owing to the influence of the slowly varying normal-mode frequencies around the saddle point region, as it is shown next.

Figure 4 shows the normal mode eigenvalue dependence on the reaction coordinate s. The connection between adjacent eigenvalues has been done according to the maximum overlap criterium, i.e., following a diabatic approach for the normal-mode frequency change (conversely, connecting the eigenvalues by a strict energy ordering along s corresponds to an adiabatic following, so that the crossings should be changed to a set of avoided crossings). The present system has nine normal modes, two of them lying much higher in energy both in the reactant

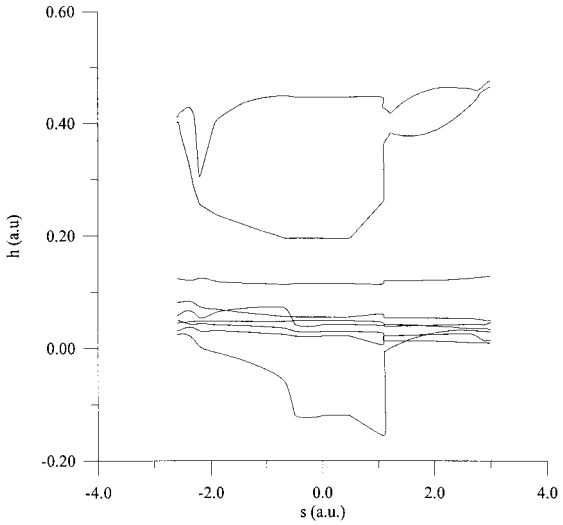

Figure 4. Normal mode eigenvalue dependence on *s*. It is obtained from the Hessian diagonalization, corresponding to each of the quadratic expansions of the potential, and further connecting diabatically adjacent eigenvalues, according to the maximum overlap of the corresponding eigenvectors.

and product configurations. Normal modes 1 and 8 (the numbering being dictated by the energy ordering in the reactant configuration) are stabilized substantially when approaching the saddle point, whereas the remaining modes are much less affected. Their frequencies become higher again when reaching the product region. It then appears that both reactant modes 1 and 8 are those more affected by the rearrangement process and thus those having a major role in the detailed reaction mechanism. Abrupt changes in some of the normal-mode frequencies are observed at an *s* value of aproximately 1.1. They arise as a consequence of the first bifurcation point described above, i.e., an abrupt change in the potential features as the IRC is followed. Stability of the dynamical solutions was carefully tested across this PES region. The step size was reduced around that region, the final results being again invariant. We then conclude that, despite the sudden change in the characteristics of the associated motion across the bifurcation region, the present methodology is able to deal with it. The problem of going across these regions is thus limited to the IRC following algorithms, an issue that is not checked at present.

At this point, a more complete picture of the reaction mode should be gained from the analysis of the whole set of normal mode dynamics. The first issue is to provide some rationale for the normal-mode frequency change on *s*. The lowermost frequency in Figure 4 corresponds to an out-of-plane $H_5-C_1-C_2$ bend (the atom numbering is given in Figure 1, whereas the reference plane is that defined by $C_1-C_2-O_3$), which is common to the reactants, products, and TS configurations. In the reactants configuration, H_4 describes also a bending motion, with respect to C_1 and C_2, being in phase with H_5. In the products configuration, conversely, H_4 bends out of phase with H_5. Finally, in the TS configuration H_4 describes a vibration, between the C_1 and C_2 atoms and parallel to the C_1-C_2 bond, on a plane parallel to that defined by $C_1-C_2-O_3$ and located below it. The frequency decrease is then explained in terms of the weakening of the C_2-H_4 and C_1-H_4 bonds, as one moves from the minima toward the TS. Figure 5 depicts the corresponding normal mode vectors for reactants, transition state, and products normal mode 1. A similar analysis can be performed for mode 8. It corresponds essentially to an H−C stretch, the hydrogen being H_4 for products and TS, whereas both H_4 and H_5 describe stretching vibrations for reactants. As

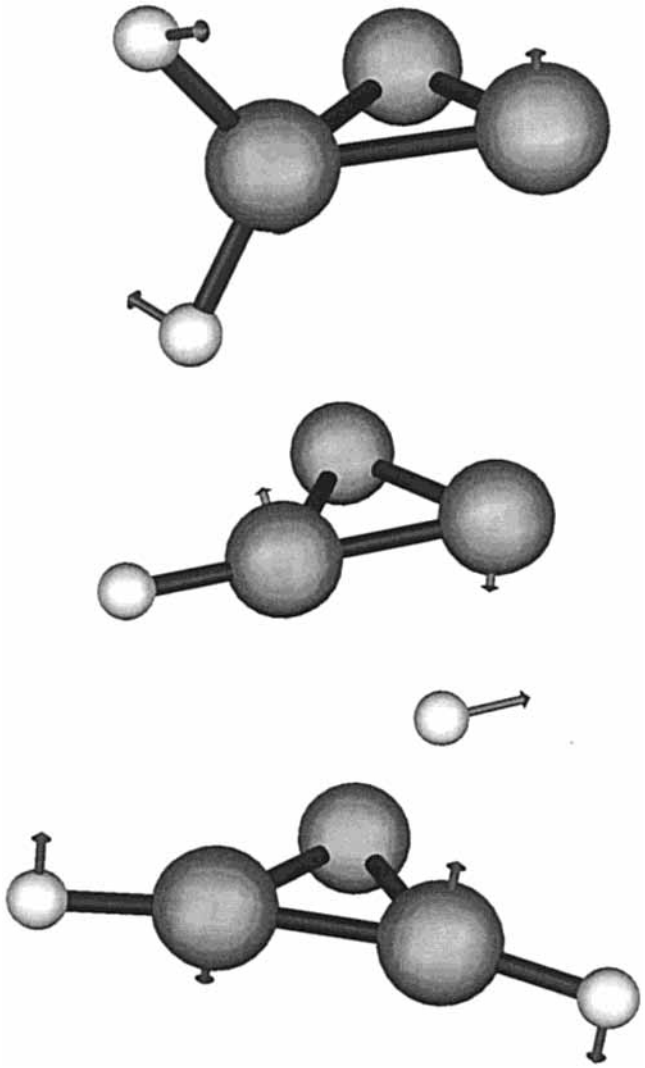

Figure 5. Normal mode vectors associated with the lowermost frequency of Figure 4, for (a) reactants, (b) transition state, and (c) products configurations, respectively.

for the TS configuration, the H_4 vibration takes place on a line perpendicular to the $C_1-C_2-O_3$ plane and below it. Its lower frequency, compared to both reactants and products, is seen clearly, thanks to the partial bending character of this H_4 vibration, if considered with respect to the C_1-H_4 and C_2-H_4 bonds. Mode 9 corresponds again to essentially a C−H stretch. However, its frequency is much less affected by the IRC potential profile, since it involves the H_5 atom, which clearly acts as a "spectator" during the rearrangement process. Finally, the remaining normal modes (2−7) are less affected by the potential profile because they correspond mainly to "breathing" modes of the $C_1-C_2-O_3$ frame, which is again almost unaltered by the unimolecular rearrangement.

The above normal-mode features are driven by the potential energy, in particular by its change on the whole set of normal mode coordinates, as one advances along the arc length *s*. It provides a structural description of the rearrangement process plus some indications on how the vibrational frequencies participate in that process. However, the description of the reaction mechanism is not complete without explaining how the energy stored in the nuclear degrees of freedom floats among them during the course of the reaction. An indication on how this energy flow among modes takes place is given in Figure

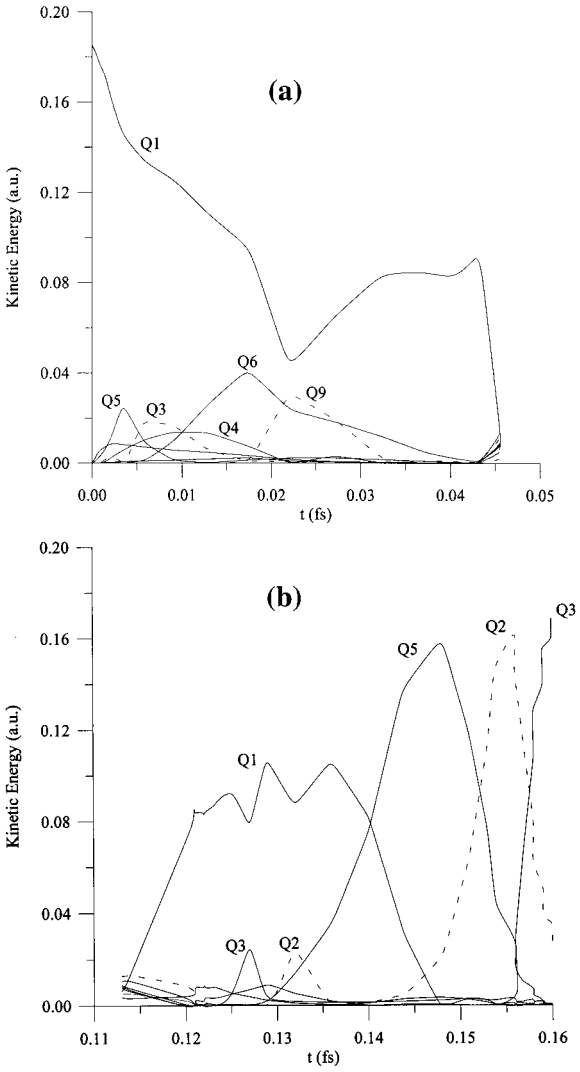

Figure 6. Kinetic energy stored in each normal mode, as a function of time, for (a) reactant and (b) product regions. The splitting of the overall time dependence into two parts has been done in order to ease the analysis of the initial and final stages, where most of the intramolecular mode couplings take place.

6, where the kinetic energy stored in each normal mode is plotted as a function of time. This quantity is easily available (analytical inside each quadratic sector) from the main equations of the present model, this being one of its advantages.

The overall shape of each trace in Figure 6 tells that potential energy captures most of the initial and final kinetic energy around the TS region, as required by total energy conservation. Actually, the "initial" conditions necessary for solving the dynamical equations are determined, in the present method, at the TS. They have been presently chosen as following an exponentially decreasing distribution of kinetic energies among the whole set of normal modes according to their normal-mode frequency at $s = 0$ (the squared modulus taken for the imaginary frequency). The way the kinetic energy changes before and after the TS, the quantity of concern here, is far from simple, providing insight on the energy transfer mechanism, which otherwise remains unnoticed from inspection of just the IRC features. Thus, the isomerization process starts from an initial state that concentrates almost all kinetic energy on the isomerization mode, Q_1, pointing out an important selectivity. As the process goes on, part of this energy flow describes a kind of "trajectory", going through Q_5, Q_3, Q_4, Q_6, and Q_9, by means of successive excitations and deexcitacions of these modes. They act as simple energy mediators because the process further advances with Q_1 capturing again a major part of the available kinetic energy. It is interesting to emphasize that the above energy transfer does not take place randomly among the "breathing" C−C−O modes, but rather it describes a well-defined pattern, as stated, of successive excitations and de-excitations. Just before the TS, most of the kinetic energy is converted into electronic potential energy, by virtue of the uphill advance of the isomerization process.

As the TS is overcome toward the product minimum, Q_1 acquires again almost all of the kinetic energy released by the potential. During this energy acquisition, a lowly effective energy transfer between Q_1 and Q_3, Q_2 takes place, which is quickly returned to Q_1. At about 0.14 fs, however, a nearly quantitative, stepwise transfer takes place, by which the Q_5, Q_2, and finally Q_3 are successively excited and deexcited, except for the latter, which is the vibration mode mostly excited at the end of the isomerization process. This indicates an important specificity in the process here described. Overall, both the reactants-to-TS and TS-to-products motions display C−H bend to C−C−O breathing mode transfer, taking place at intermediate times for the former and at final times for the latter.

The present results are, of course, dependent on the initial conditions. In the present method they are determined, as stated, at the transition state. Further knowledge of this process requires considering a representative set of initial conditions, i.e., a proper distribution in phase space, so as to get typical kinetic quantities such as rate constants. This extended analysis, along with further extensions to angular momentum based formulations, as well as semiclassical and quantum mechanical versions, is left for future work.

V. Summary and Conclusions

An implementation of the RPH Hamiltonian of Miller, Handy, Adams, based on an explicit relation between the set of internal coordinates and the IRC arc length, has been presented. This relation originates from a first order expansion of the gradient. The result is that both the kinetic and potential energy functions are dependent on the arc length distance plus the gradient and Hessian along it. The ultimate consequence is that the unique dynamic equation for the complete system can be solved efficiently in two stages. First, the arc length time dependence, $s(t)$, is obtained from a second-order Bernouilli-type equation, having the gradient vectors and Hessian matrices along the arc length as input data. This equation is solved analytically inside the validity range of quadratic expansions of the potential, centered on successive points of the reaction coordinate. The whole time dependence is afterward recovered, stepwisely, from the continuity conditions between adjacent quadratic expansions. The second stage leads to the full normal mode time dependence, starting from $s(t)$, the gradients, and Hessians for each quadratic expansion, and the overlaps between adjacent quadratic expansion eigenvector matrixes.

The result is a computationally efficient ab initio direct dynamics method, thanks to a previous assembling of the dynamical code with an adequate quantum chemistry package. The possibilities of the present method have been illustrated, in this work, studying the 1,2 hydrogen migration between the (corresponding) carbene and ethyne oxide, a 9-normal mode problem. Especially appealing is the straightforward analysis emerging from the simultaneous use of the frequency dependence on the reaction coordinate and the time evolution of the kinetic energy captured by each normal mode. In particular, the present system shows both an important isomerization

selectivity and specificity, since it concentrates most of the initial and final energy in the isomerization mode, Q_1, and a breathing mode, Q_3, respectively. In addition, some of the frame modes act as necessary energy mediators during the time evolution in the reactants region. And, furthermore, the process ends up with a nearly quantitative, stepwise vibrational energy transfer between Q_1 and Q_3, through mediation of the Q_5 normal mode.

The method is presently restricted to the strictly classical problem, which might be of use for making more efficient dynamics studies of very large molecular systems. Further improvements may consist of developing suitable semiclassical or quantum mechanical versions of it, as well as its use for rate constant calculations and related quantities. A major reason for putting some effort in this method is that the use of a RPH-type coordinate system appears well adapted, in principle, for dealing with the multidimensional initial condition sampling problem, present when these latter quantities are required. All of these possibilities are being actively pursued in our laboratory.

Acknowledgment. We are indebted to Professors S. Olivella and A. Aguilar for valuable suggestions. This research was supported by the Spanish DGICYT (Grants PB98-1240-CO2-01 and PB97-0919). J.G. acknowledges the CeRQT (Universitat de Barcelona), for a predoctoral fellowship.

References and Notes

(1) See, for instance, (a) *Faraday Discuss. Chem. Soc.* Chemical Reaction Theory **1998**, *110*. (b) *Phys. Chem. Chem. Phys.* Special Issue Chemical Reaction Theory **1999**, *1*. (c) *Phys. Chem. Chem. Phys.* Special Issue **2000**, *2*.

(2) (a) Hofacker, G. L. *Z. Naturforsch. A* **1963**, *18*, 607. (b) Marcus, R. A. *J. Chem. Phys.* **1966**, *45*, 4493, 4500. Marcus, R. A. *J. Chem. Phys.* **1968**, *49*, 2610.

(3) Miller, W. H.; Handy, N. C.; Adams, J. E. *J. Chem. Phys.* **1980**, *72*, 99.

(4) Miller, W. H. *J. Phys. Chem*. **1983**, *87*, 3811.

(5) For recent work see, for instance, (a) Fang, J.-Y.; Hammes-Schiffer, S. *J. Chem. Phys.* **1998**, *109*, 7051, and references therein. (b) Hu, H.; Kobrak, M. N.; Xu, Ch.; Hammes-Schiffer, S. *J. Phys. Chem. A* **2000**, *104*, 8058.

(6) Nguyen, K. A.; Jackels, C. F.; Truhlar, D. G. *J. Chem. Phys.* **1996**, *104*, 6491, and references therein. Also, The reaction path in chemistry: current approaches and perspectives in *Understanding chemical reactivity;* Heidrich, D., Ed.; Kluwer: Dordrecht, 1995; Vol. 16.

(7) Heller, E. J. *J. Chem. Phys.* **1975**, *62*, 1544.

(8) Millam, J. M.; Bakken, V.; Chen, W.; Hase, W. L.; Schlegel, H. B. *J. Chem. Phys.* **1999**, *111*, 3800.

(9) Fukui, K. *Acc. Chem. Res*. **1981**, *14*, 363.

(10) Gonzalez, C.; Schlegel, H. B. *J. Phys. Chem*. **1990**, *94*, 5523.

(11) Quapp, W.; Heidrich, D. *Theor. Chim. Acta* **1984**, *66*, 245.

(12) Wilson, E. B.; Decius, G. C.; Cross, P. C. *Molecular Vibrations*; McGraw-Hill: London, 1955.

(13) Sun, J. Q.; Ruedenberg, K. *J. Chem. Phys*. **1993**, *98*, 9707.

(14) McKelvey, J. M.; Hamilton, J. F. *J. Chem. Phys*. **1984**, *80*, 579.

(15) Page, M.; McIver, J. W. *J. Chem. Phys*. **1988**, *88*, 922.

(16) Ischtwan, J.; Collins, M. A. *J. Chem. Phys*. **1988**, *89*, 2881.

(17) (a) Sun, J. Q.; Ruedenberg, K. *J. Chem. Phys*. **1993**, *99*, 5257. (b) Sun, J. Q.; Ruedenberg, K. *J. Chem. Phys*. **1993**, *99*, 5269. (c) Sun, J. Q.; Ruedenberg, K.; Atchity, G. J. *J. Chem. Phys*. **1993**, *99*, 5276. (d) Ruedenberg, K.; Sun, J. Q. *J. Chem. Phys*. **1994**, *100*, 6101.

(18) Fletcher, R. *Practical Methods of Optimization*; Wiley: New York, 1987.

(19) See, e.g., Arnold, V. I. *Métodos Matemáticos de la Mecánica Clásica*, MIR: Moscú, 1997 (spanish translation of the 1984 russian version).

(20) Aleksandrov, A. D.; Kolmogorov, A. N.; Laurent'ev, M. A. *Mathematics, its content, methods and meaning*; Dover: New York, 1999.

(21) Schlegel, H. B. In *Modern Electronic Structure Theory*; Yarkony, D. R., Ed.; World Scientific: Singapore, 1995; p 459.

(22) Bofill, J. M. *J. Comput. Chem*. **1994**, *15*, 1.

(23) Bofill, J. M.; Comajuan, M. *J. Comput. Chem*. **1995**, *16*, 1326.

(24) Bakken, V.; Millan, J. B.; Schlegel, H. B. *J. Chem. Phys.* **1999**, *111*, 8773.

(25) Culot, P.; Dive, G.; Nguyen, V. H.; Ghuysen, J. M. *Theor. Chim. Acta* **1992**, *82*, 189.

(26) Helgaker, T.; Uggerud, E.; Jensen, H. J. A. *Chem. Phys. Lett*. **1990**, *173*, 145.

(27) Sun, J. Q.; Ruedenberg, K. *J. Chem. Phys*. **1994**, *101*, 2157.

(28) Schröder, S.; Thiel, W. *J. Am. Chem. Soc.* **1985**, *107*, 4422.

(29) Bouma, W. J.; Nobes, R. H.; Radan, L.; Woodward, C. E. *J. Org. Chem.* **1982**, *47*, 1869.

(30) Dewar, M. J. S.; Thiel, W. *J. Am. Chem. Soc*. **1977**, *99*, 4899.